Key Engineering Materials
ISSN: 1662-9795, Vol. 924, pp 93-104
doi:10.4028/p-at3rx9

Submitted: 2021-09-28
Revised: 2022-03-20
Accepted: 2022-03-26
Online: 2022-06-30

The Influence of Material Position Towards the Bending Strength of the 4 Pass AA1050/AA6082 and AA6082/AA1050 FSPed Joints

Oritonda Muribwathoho[1,a], Velaphi Msomi[1,b], Sipokazi Mabuwa[1,c]

[1]Cape Peninsula University of Technology, Mechanical Engineering Department, 7535, South Africa.

[a]oritondamuribwathoho@gmail.com, [b]msomiv@gmail.com, [c]sipokazimabuwa@gmail.com

Keywords: Aluminium alloy, tensile properties, microhardness, bending strength, microstructural analyse, friction stir processing and friction stir welding.

Abstract. This paper reports on the influence of material position towards the bending strength of the 4 pass AA1050/AA6082 and AA6082/AA1050 FSPed joints. FSW approach was utilized to create dissimilar joints using two dissimilar plates. After that, the created dissimilar joints were put through a multi-pass friction stir processing. The microstructural analysis results revealed that the 4P 6082/1050 joint had substantially finer grains than the 4P 1050/6082 joint. The 4P 1050/6082 joint yielded the highest ultimate tensile strength when compared to that of the 4P 6082/1050 joint . The Vickers microhardness of 1050/6082 FSPed joints was found to be increased towards the AA6082, while 6082/1050 FSPed joints decreased towards AA1050. The bending strength analysis showed that there was no obvious trend in flexural strength.

1. Introduction

Friction Stir Processing (FSP) is an advanced process for altering the microstructure of a processed alloy [1], which leads to the structure rearrangement and grain size alteration, which has already been developed through the use of the Friction Stir Welding (FSW) technique, that was introduced by TWI Ltd in the United Kingdom in 1991. Material flow affecting parameters such as material positioning, process parameters, tool design, and process improvements are essential for the overall performance of friction-based manufacturing processes like friction stir welding, friction stir lap welding and friction stir spot welding [2,3,4,5,6,7,8,9,10,11,12].

According to the literature, using a softer aluminum alloy on the advancing side promotes higher material flow and, as a result, better weld performance. Some research suggests that putting the hardest material on the advancing side might enhance the heat input while welding [13-15]. Lee et al. [16] analyzed the joint properties of dissimilar Al alloys formed by friction stir welding according to the fixed location of materials and concluded, based on the results, that the joint properties are strongly dependent on the alloy on the retreating side, because the stir zone is composed mainly of the retreating side material. Jeon et al. [17] analyzed the material properties of friction stir spot welded joints of dissimilar aluminum alloy and observed that material position was not a key fracture influencing parameter in friction stir spot welded 5052-H32/6061-T6 joints, but hook defect was a significant stress raiser, independent of Al alloy arrangement.

According to numerous studies, high strength material should be positioned on the advancing side of the dissimilar junction to improve mechanical characteristics [18–20]. Cavaliere et al. [21] studied the effect of welding parameters on mechanical and microstructural properties of dissimilar AA6082–AA2024 joints produced by friction stir welding. They observed that maximum fatigue behavior in the AA6082-AA2024 joint occurs when a higher strength material (AA2024 Aluminim alloy) is positioned on the advancing side, but an inherent forging flaw induced fracture start in the AA2024-AA6082 joint (AA2024 at the advancing side). The impact of materials positioning on the microstructure of friction stir processed dissimilar joints was investigated by Msomi and Mabuwa [22]. They observed that when the stronger material is positioned on the advancing side, the ultimate tensile strength and yield strength improved, but when the low strength material is positioned on the advancing side, the percentage elongation improved dramatically.

Paidar et al. [23] investigated the effects of material position on dissimilar modified friction stir clinching of AA2024-AA6061 aluminum alloys and found that the AA2024-T3/AA6061-T6 joint is stronger than the AA6061-T6/AA2024-T3 joint. Pabandi et al. [24] studied effect of precipitation hardening heat treatment on mechanical and microstructure features of dissimilar friction stir welded AA2024-T6 and AA6061-T6 alloys and found that when AA6061-T6 Al alloy was placed on the advancing side of AA2024-T6 and AA6061-T6 Al alloys during friction stir welding there was appropriate plastic material inter-mixing and better tensile strength.

Mabuwa and Msomi [25] investigated the effect of friction stir processing on the mechanical properties of friction stir welded AA1050-H14 and AA6082-T6. They discovered that when AA1050-H14 is placed on the advancing side while AA6082-T6 is placed on the retreating side for both FSW and FSP joints, the mechanical properties are higher than when the weak alloy is placed on the retreating side, implying that when welding dissimilar alloys the material positioning has an impact on the outcomes.

The influence of material position on friction stir welding dissimilar joints is mostly reported in the literature, however there is limited study on the effect of material position on dissimilar joint processing. The literature reveals that material position is an important factor to consider during the FSP technique. It is not quite clear if the material position affects bending strength of the joint formed from dissimilar materials. This research is essential since there is a limited literature in this subject. This study reports on the influence of material position on the bending strength of the 4 Pass AA1050/AA6082 and AA6082/AA1050 FSPed joints.

2. Materials and Methods

The two selected plates AA1050-H14 and AA6082-T651 were cut into the FSW/FSP LAGUN FA.1-LA (semi-automated milling machine) backplate's required sizes. The dimensions of the dissimilar plates are 260 x 52 mm with a thickness of 6 mm. FSW was utilized to form a dissimilar joint 1050/6082 and 6082/1050 using the dimensioned plates. The FSWed plates were further subjected to 4 pass multi-pass friction stir processing. Figure 1(a) and (b) shows the FSWed plates. Figures 1 (c) and (d) illustrate the FSPed plates. The tool utilized in this experiment was high-speed tool steel with 5.8 mm pin length and 8 mm diameter. The tool's shoulder diameter was 20 mm. It should be emphasized that the FSW technique used the same parameters, equipment, and setup as the FSP process, and that it was based on earlier research [26-27]. It's also worth remembering that 1050/6082 means that AA1050 was on the advancing side and 6082/1050 implies that AA6082 was on the advancing side during FSW and FSP. The chemical composition of AA1050 is 0.16 wt.% Si, 0.66 wt.% Fe, 0.03 wt.% Cu, 0.12 wt.% Mn, 0.60 wt.% Mg, 0.07 wt.% Ni, 0.56 wt.% Zn, 0.02 wt.% Ti, 0.69 wt.% Pb, 0.02 wt.% V, 0.03 wt.% Co and 96.9 wt.% Al. The chemical composition of AA6082 is 0.33 wt.% Si, 0.43 wt.% Fe, 0.02 wt.% Cu, 0.35 wt.% Mn, 1.09 wt.% Mg, 0.05 wt.% Ni, 0.32 wt.% Zn, 0.01 wt.% Ti, 0.39 wt.% Pb, 0.0 wt.% V, 0.01 wt.% Co and 97.0 wt.% Al.

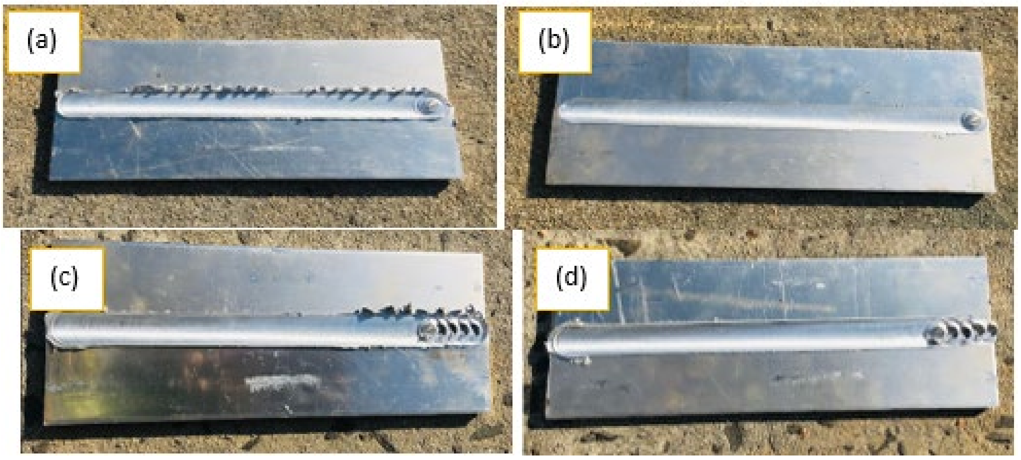

Figure 1: FSWed Plate; (a) AA1050 on the advancing side, (b) AA6082 on the advancing side, FSped Plate; (c) 4P FSPed 1050/6082 and (d) 4P FSPed 6082/1050.

The FSPed plates were cut in preparation for different tests. SEM was used to examine the fracture type of the post-tensile test specimens. Motic AE2000 microscope was used to carry out the microstructural analysis. Keller's and Weck's reagents were modified to create etchants for microstructural analysis to reveal the AA1050 and AA6082 grains. The etching procedure is the same as that employed previously in the literature [22,25,26-31]. ImageJ software was used to calculate the average grain size according to the ASTM E112-12 standard. The Hounsfield 50 K testing machine was used to conduct the tensile and bending tests. The ASTM-E8M-04 standard was utilized to determine the geometry of the tensile specimen and to conduct the tensile test. The ASTM E290 standard was used to generate the bending specimen design and geometry. Figure 2 (a) shows a schematic representation of the tensile specimen utilized in this investigation. Figure 2 (b) depicts the schematic diagram for the bending specimen. Microhardness was determined utilizing an Innova Test (Falcon 500) equipment and ASTM E384-11. Figure 2(c) illustrates the schematic diagram for the microhardness specimen. The specimen sample locations are shown in Figure 2(d) on the FSPed plate after the specimens have been removed. S denotes the start, M denotes the middle and E denotes the end of the joint.

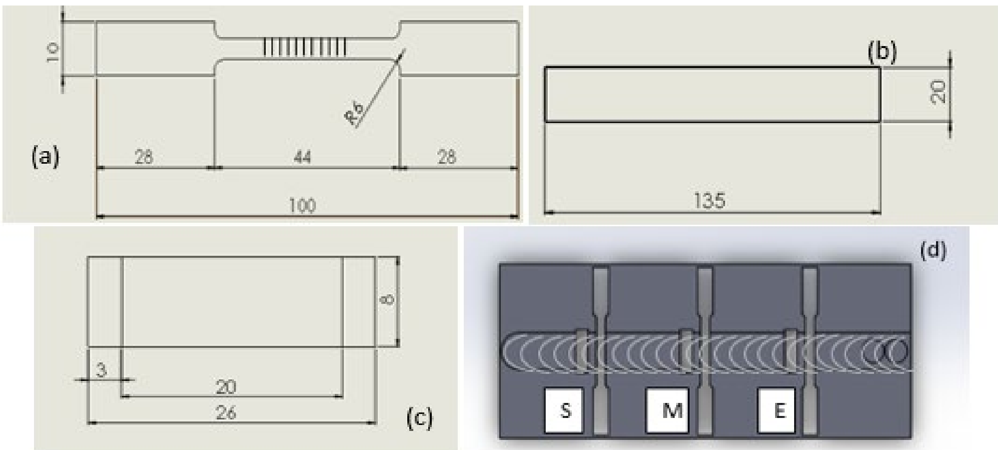

Figure 2: (a) Tensile test specimen, (b) Bending specimen, (c) Microhardness specimen (all the dimensions are in mm), (d) Specimen positions on FSPed sampled plate.

3. Results and Discussion

3.1 Metallographic morphology

The microstructural morphology of the stir zone (SZ) for 4P FSPed joints was captured using optical microscopy. Figure 3 (a) - (c) depicts the SZ microstructural grain arrangement of specimens obtained at the S, M, and E for the 4P 1050/6082, whereas figures 3 (d), (e), and (f) show the SZ microstructural grain arrangement of specimens collected at the S, M, and E for the 4P 6082/1050. The linear intercept approach was employed to measure the grain size of each specimen using ImageJ software. For the 4P 1050/ 6082 and 4P 6082/1050 FSPed joints, table 2 summarizes the average grain size measurements of the mean grain sizes, standard deviations, minimum and maximum grain sizes of the surfaces depicted in Figure 3. The 4P 1050/6082 mean grain size joint ranged from 5.381 to 9.120 µm, while the 4P 6082/1020 mean grain size ranged from 1.744 to 1.193 µm. The standard deviation for the 4P FSPed 1050/6082 was 1.599 to 2.245 µm, while the standard deviation for the 4P FSPed 6082/1050 was 0.320 to 0.351 µm. As a result of dynamic recrystallization in the SZ, the 4P FSPed 1050/6082 joint and 6082/1050 joint surfaces exhibited equiaxed grains with high angle grain boundaries. Dynamic recrystallization occurred as the number of FSP passes increased, causing grain size refinement. The extreme heat generated during processing contributes significantly to equiaxed grain sizes [32,33,34].

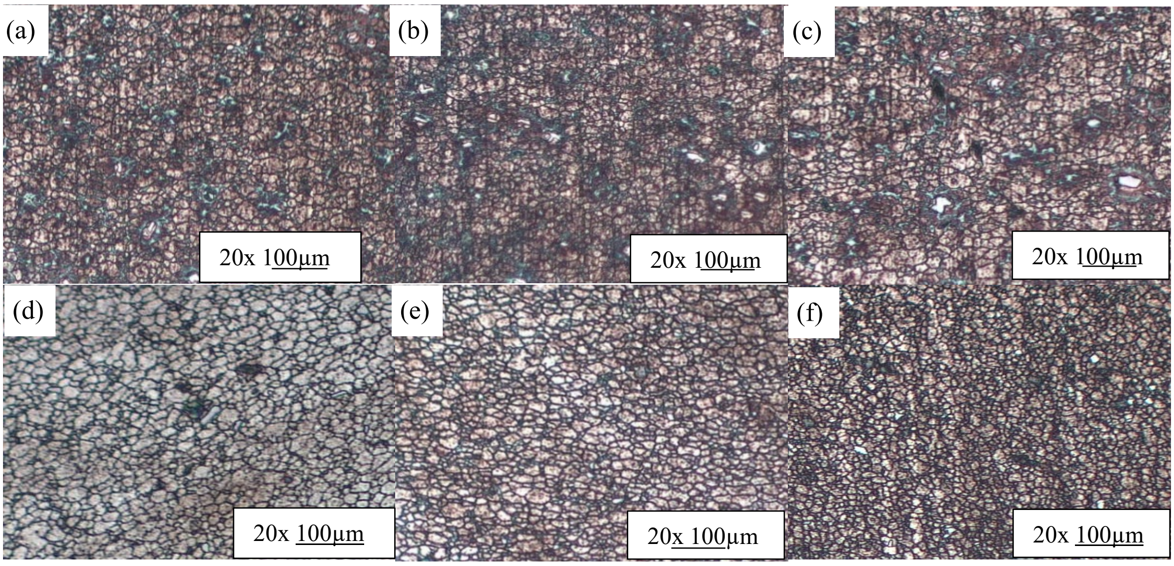

Figure 3: Micrographs (1050/6082); *4* pass FSPed (a) S, (b) M, (c) E ;Micrographs (6082/1050); *4* pass FSPed (d) S, (e) M, (f) E

Table 2: Average grain measurements

Material positioning	**Mean Values [µm]**	**Standard Deviation**	**Minimum**	**Maximum**
4P 105/6082				
Start	9.120	2.245	6.250	13.80
Middle	8.804	1.971	6.250	13.75
End	5.381	1.599	2.560	9.874
4P 6082/1050				
Start	1.193	0.351	1.913	2.479
Middle	1.443	0.335	1.235	2.469
End	1.744	0.320	1.274	2.297

3.2 Tensile Properties

Figures 4 (a) and (b) show the post-tensile specimens for a 4P 1050/6082 joint and a 4P 6082/1050 joint, respectively. Figures 4 (c) and (d) show bar graphs of ultimate tensile strength and % elongation for specimens taken from various places for each friction stir processed joint, such as the beginning, middle, and end of the joint, respectively. Tensile properties for the base material used for this study are the same used in the literature [22, 26-27]. The specimen sampled at the joint's end yielded the highest UTS of 86.1 MPa for the 4P 1050/6082 joint. The specimen sampled at the joint's middle yielded the highest UTS of 69.5 MPa for the 4P 6082/1050 joint. From the beginning to the end of the 4P 1050/6082 FSPed joints, the UTS increased, whilst the % elongation dropped from the S to the E. A decrease in grain size at the 4P 1050/6082 junction causes this behavior [25,35]. The 4P 6082/1050 joint FSPed joints' ultimate tensile strength (UTS) was seen to vary from the S to the E of the joint. The % elongation decreased from the beginning to the end of the 4P FSPed joints. All of the 4P FSPed joints' UTS were lower than the base metals', a tendency that had previously been seen in the literature [26-27,36].

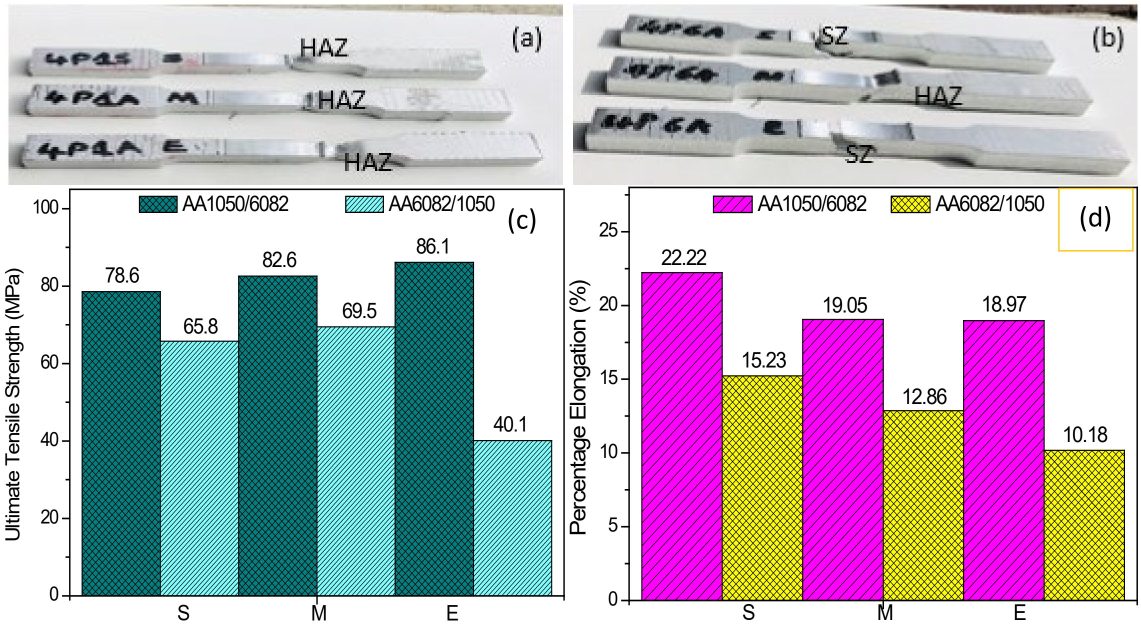

Figure 4: Post tensile specimens (4P FSPed joints); (a) 1050/6082; (b) 6082/1050; 4P FSPed joints bar graphs: (c) Ultimate tensile strength and (d) Percentage elongation

3.2.1 Tensile Surface Morphology (SME)

Figure 5 (a)-(c) depicts the fractographic surface morphology of specimens obtained from the S, M, and E of 4P 1050/6082. Figure 5 (a)- (c) depicts the fractographic surface morphology of specimens obtained from the S, M, and E of 4P 6082/1050. The dimples and microvoids on the fractured surface of the 4P 1050/6082 FSPed joints defined it, as shown in figure 5 (a) - (c). All 4P FSPed 1050/6082 joints showed ductile trans-granular failure. The presence of dimples and microvoids on the morphology indicates a ductile failure mode [37-38]. As illustrated in figure 5 (d)- (f), the 4P 6082/1050 FSPed joints were characterized by the presence of river-like fractured surfaces, dimples cracked surfaces, microvoids, and flat surfaces. The presence of river-like structures on the morphology indicates inadequate materials mixing or a joint that has been subjected to significant heat input, which is usually indicated by fracture at the stir zone [39-42]. Micro-voids and dimples cracked surfaces are visible in Figure 5 (e). Figures 5 (d) and (f) show the presence of river-like fragmented surfaces with ductile failure mechanisms. The presence of dimples paired with flat structures on the fractured surface of the 4P 6082/1050 specimen indicates ductility mixed with brittleness.

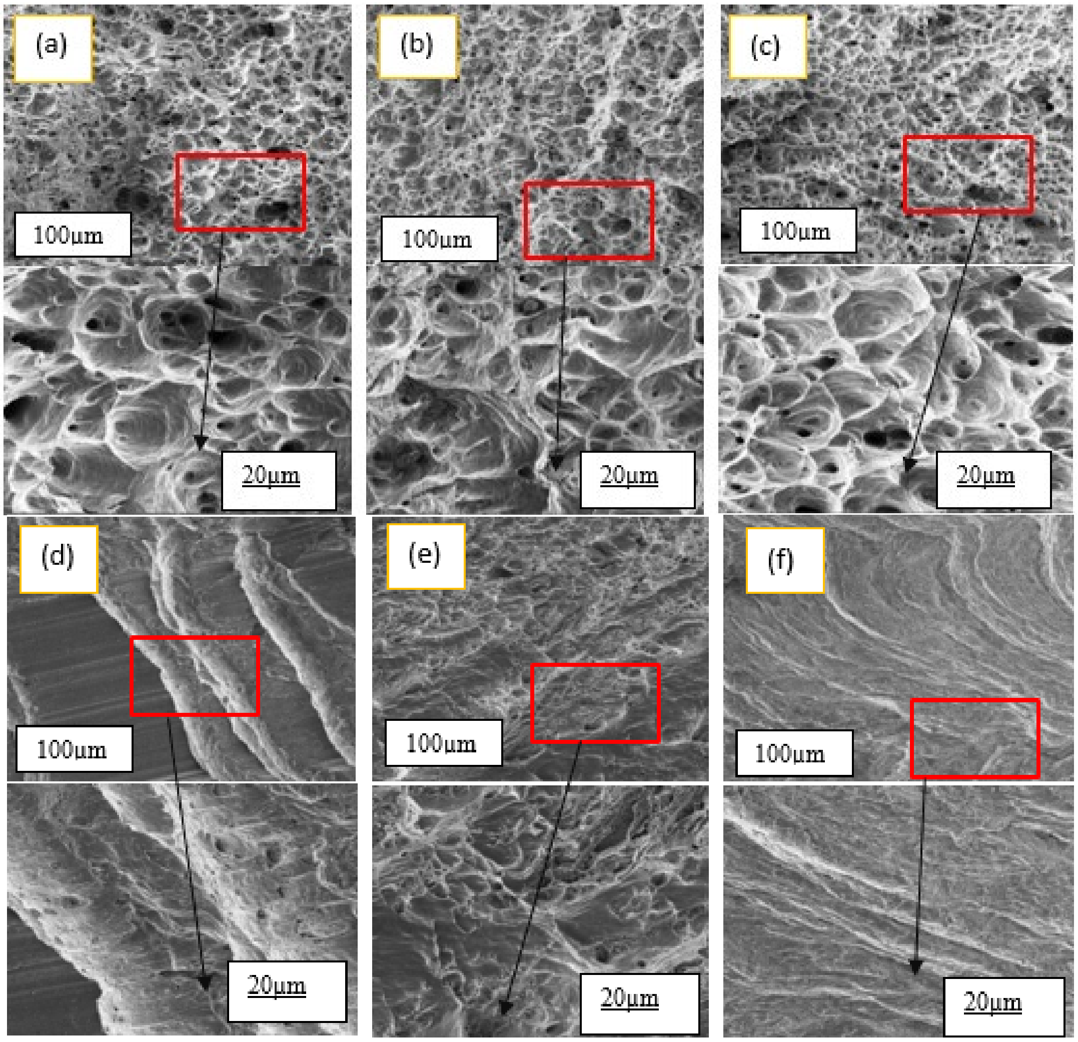

Figure 5: SEM tensile 4P FSPed 1050/6082; (a) S, (b) M. (c) E;
SEM tensile 4P FSPed 6082/1050; (d) S, (e) M. (f) E

3.3 Microhardness

The Vickers microhardness values for the FSPed joints are shown in Figure 6. Microhardness profiles for specimens collected at the S, M, and E of the 4P 1050/6082 and 4P 6082/1050 joints, respectively, are shown in Figure 6 (a) and (b). The 4P 1050/6082 joint's SZ Vickers microhardness varied from 23.33 to 57.14 HV from start to end, with the maximum SZ microhardness of 57.14 HV measured on the middle specimen sample. From start to end, the SZ Vickers microhardness of the 4P FSPed joint varied between 40 and 59.6 HV, with the maximum microhardness of 59.6 HV recorded on a specimen sample taken from the center of the 4P 6082/1052 joint. With AA1050 on the advancing side, the TMAZ microhardness on the advancing side's is lower than on the retreating side's, but when AA6082 is on the advancing side, the advancing side's TMAZ microhardness is greater than the retreating side's and so on. The 4P 1050/6082 FSPed joint's microhardness increased as it neared the AA6082, whereas the 4P 6082/1050 FSPed joint's microhardness reduced as it reached the AA1050. The thermal cycle in which the strengthening precipitates dissolve and coarsen causes the drop in hardness while 6082 is on the advancing side [43]. The precipitation and nucleation of thick intermetallic compounds induced by high temperature and high deformation rate are related with a rise in microhardness while AA1050 is placed in the advincing side [44-46].

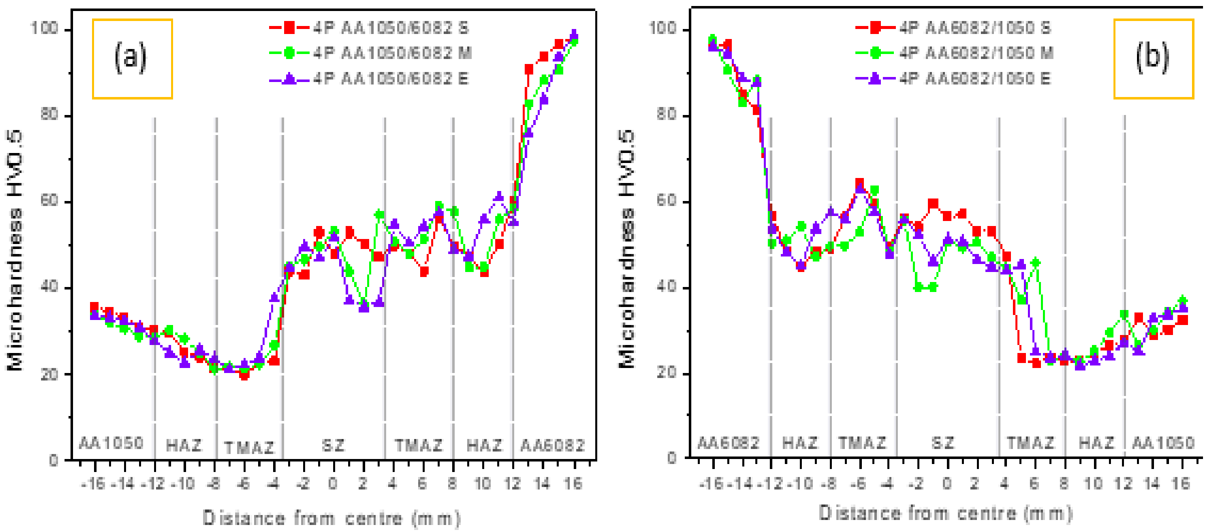

Figure 6: Microhardness results: (a) 4P 1050/6082 (b) 4P 6082/1050

3.4 Bending Strength

Figures 7 (a) – (d) show the post flexural test specimens for the 4P 1050/6082 FSPed joints and the 4P 6082/1050, FSPed joints. Figure 7 shows the post-flexural test specimens for the roots (a) for 4P 1050/6082 and (b) for 4P 6082/1050, as well as the post-flexural test specimens for the face (c) for 4P 1050/6082 and (d) for 4P 6082/1050. For the FSPed joints, it was discovered that the roots and face specimens failed at different locations. Some joints were free of cracks after a maximum deflection, while others showed evident cracks. Figure 7 (e)- (h) shows the flexural stress and strain curves of friction stir treated joints. The root stress and strain curves for the specimens are shown in Figure 7: (e) for the 4P 1050/6082 and (f) for the 4P 6082/1050. The specimen's stress and strain curves for the face are shown in Figure 7: (g) for the 4P 1050/6082 and (h) for the 4P 6082/1050. The 4P 1050/6082 Fsped joint's root and face flexural highest strengths were 298.5 MPa and 281.25 MPa, respectively. The highest flexural strength was found at the start of the joint for the root, and in the middle of the joint on the 4P 1050/6082 for the face. The 4P 6082/1050 FSPed joint had the highest root and face flexural strengths of 276.94 MPa and 226.5 MPa, respectively. The 4P 6082/1050 the end of the joint had the highest root flexural strength, and the highest face flexural strength was also at the end of the joint.

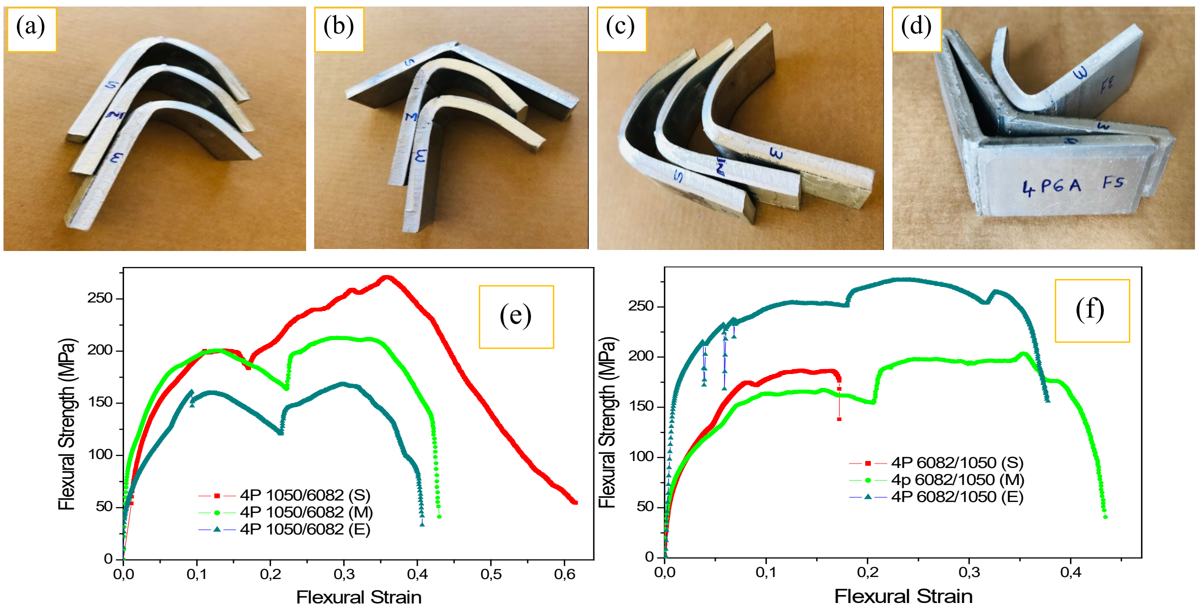

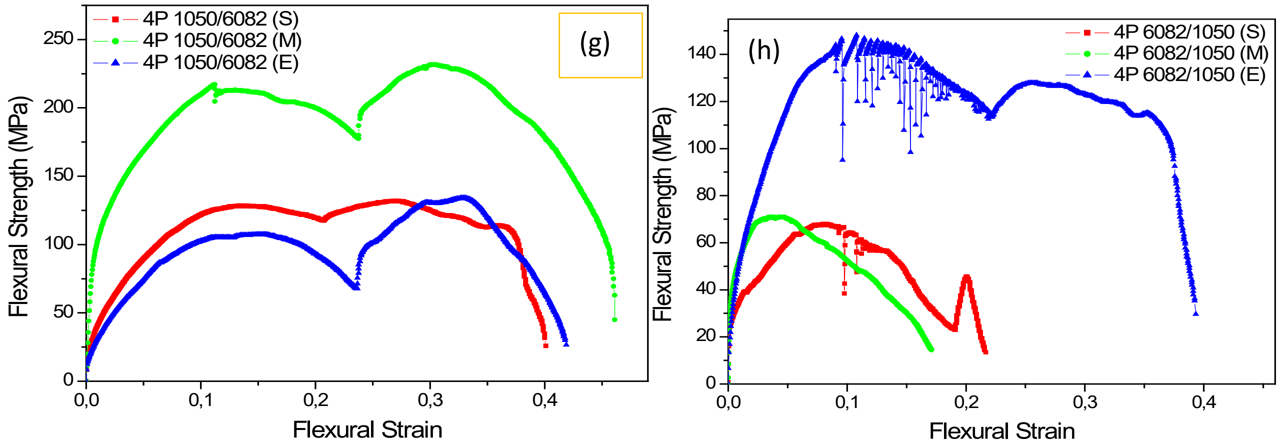

Figure 7: Post flexural test specimens; (a) 4P 1050/6082 (Root), (b) 4P 6082/1050 (root), (c) 4P 1050/6082 (Face), (d) 4P 6082/1050 (Face); Flexural stress and strain curves: Root (e) 4P 1050/6082, (f) 4P 6082/1050, Face (g) 4P 1050/608 and (h) 4P 6082/1050.

Figures 8 (a) and (b) depict bar graphs of ultimate flexural strength and maximum flexural strain for the post-flexural test specimens shown in figures 7 (a) – (d). With AA6082 positioned on the advancing side, the average UFS was observed to be greater on the root side of the processed joints specimens. With AA1050 placed on the advancing side, the average MFS was noticed to be greater on the root side of the processed joints specimens. On the face specimens for the 4P 6082/1050 joint, the average MFS increased as the average UFS increased from the beginning to the end of the joint. The average UFS and MFS for the 4P 1050/6082 joint's root were found to vary. There was no clear relationship between the MFS and UFS results.

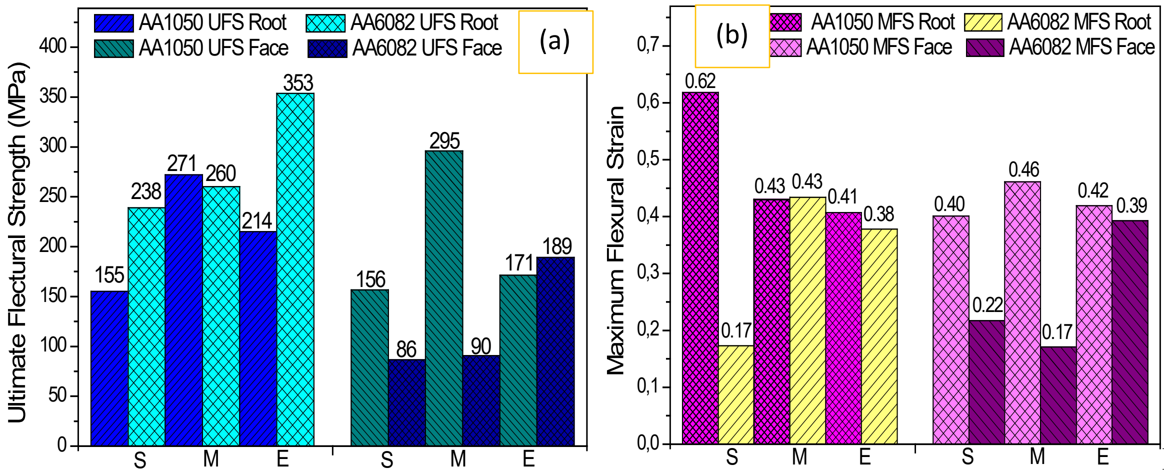

Figure 8: Bar graphs: (a) Ultimate flexural strength and (b) Maximum flexural strain.

4. Conclusions

The influence of material position towards the bending strength of the 4 pass AA1050/AA6082 and AA6082/AA1050 FSPed was studied. The results have been evaluated for the 4P FSPed joint. The following conclusions were reached based on results archived; findings are as follows:

- The grain sizes were decreased as the number of passes were increased. The grain structure was refined from 19.84 µm to 5.381 µm for 4P 1050/6082 and from 13.12 µm to 1.744 µm for the 4P 6082/1050 FSPed joints. The 4P 6082/1050 had substantially finer grains than the 4P 1050/6082.
- The 4P 1050/6082 joint's highest ultimate tensile strength was 86.1 MPa, whereas the 4P 6082/1050 joint's maximum ultimate tensile strength was 69.5 MPa.

- The microhardness of 4P 1050/6082 FSPed joints increased towards the AA6082, reaching a maximum hardness of 65.54 HV at the SZ, while the microhardness of 4P 6082/1050 FSPed joints decreased towards the AA6082 with a maximum hardness of 61.06 HV at the Sz.
- During bending test the deflection was discovered in various regions of the joints, with some joints revealing cracks and others being crack-free. During the analysis, there was no obvious trend in bending strength.

Acknowledgments

The authors would like to express their gratitude to Miranda Waldron of the University of Cape Town's SEM department for allowing them to use the SEM equipment.

Funding statement

The National Research Foundation (NRF) Thuthuka Grant [118046] was used to fund this study, which the authors gratefully acknowledge.

Data availability

On request, the data used to write this paper can be acquired from the corresponding author.

Conflict of interest

There are no potential conflicts of interest for the authors as a result of this work.

References

[1] M. Barmouz , V. Zall , H. Pashazadeh , Mechanical and Microstructural characterization of Hybrid Cu-SiC-Zn Composites Fabricated Via Friction Stir Processing, Materials Research. 19 (2016), pp.1292- 1298.

[2] W. Yuan, R.S. Mishra, S. Webb, Y.L. Chen, B. Carlson, D.R. Herling, *et al***,** Effect of tool design and process parameters on properties of Al alloy 6016 friction stir spot welds, J Mater Process Technol, 211 (2011), pp. 972-977.

[3] J. Han, R. Paidar, Vignesh, R.V, K.P, Mehta, A. Heidarzadeh, O.O. Ojo, Effect of shoulder features during friction spot extrusion welding of 2024–T3 to 6061–T6 aluminum alloys, Arch Civil Mech Eng, 20 (2020), pp.1-17.

[4] A. Heidarzadeh, S. Mironov, R. Kaibyshev, G. Çam, A. Simar, A. Gerlich, *et al,* Friction stir welding/processing of metals and alloys: a comprehensive review on microstructural evolution, Prog Mater Sci, (2020), p. 100752.

[5] Z. Shen, W.Y. Li, Y. Ding, W. Hou, X.C. Liu, W. Guo, *et al,* Material flow during refill friction stir spot welded dissimilar Al alloys using a grooved tool, J Manuf Processes, 49 (2020), pp. 260-270.

[6] L. Shi, C.S. Wu, L. Fu, Effects of tool shoulder size on the thermal process and material flow behaviors in ultrasonic vibration enhanced friction stir welding, J Manuf Processes, 53 (2020), pp. 69-83.

[7] K.K. Mugada, K. Adepu, Effect of knurling shoulder design with polygonal pins on material flow and mechanical properties during friction stir welding of Al-Mg-Si alloy, Trans Nonferrous Metals Soc China 29,11 (2019), pp.2281- 2289.

[8] Z. Sun, C.S. Wu, Influence of tool thread pitch on material flow and thermal process in friction stir welding, J Mater Process Technol, 275 (2020), p. 116281.

[9] H.A. Derazkola, F. Khodabakhshi, A.P. Gerlich, Friction-forging tubular additive manufacturing (FFTAM): a new route of solid-state layer-upon layer metal deposition, J Mater Res Technol, 9 (2020), pp. 15273-15285.

[10] H.A. Derazkola, F. Khodabakhshi, A.P. Gerlich, Fabrication of a nanostructured high strength steel tube by friction-forging tubular additive manufacturing (FFTAM) technology, J Manuf Processes, 58 (2020), pp. 724-735.

[11] M. Paidar, O. Ojo, A. Moghanian, H. Karami Pabandi, M. Elsa, Pre-threaded hole friction stir spot welding of AA2219/PP-C30S sheets, J Mater Process Technol, 273 (2019), p. 116272.

[12] S. Memon, M. Paidar, S. Sadreddini, K. Cooke, B. Babaei, O.O, Ojo, Mechanical and microstructural aspects of the hybrid joint of PP-C30S and 2219 aluminum alloy,Results Phys 19 (2020), p.103629.

[13] U. Dwivedi, S. Tiwari, A. Mishra, S. Das, Mat. Today: Proc., 22(2020).

[14] K.P. Mehta, P. Carlone, A. Astarita, F. Scherillo, F. Rubino, P. Vora, Mat. Sc. Eng. A, 759(2019).

[15] H. Mehdi, R.S. Mishra, J. Adv. Join. Proc., 1(2020).

[16] W.B Lee, Y.M. Yeon, S.B. Jung. Scr Mater 49, 5 (2003).

[17] J.E.O.N. Chi-Sung, H.O.N.G. Sung-Tae, K.W.O.N. Yong-Jai, C.H.O. Hoon Hwe, H.N. Han, Material properties of friction stir spot welded joints of dissimilar aluminum alloy, Trans Nonferrous Met Soc China, 22 (2012), pp. 605-613.

[18] S. Hassanifard, H. Alipour, A. Ghiasvand, A. Varvani-Farahani, J. Manuf. Proc., 64(2021).

[19] A. Fall, H. Monajati, A. Khodabandeh, M.H. Fesh araki, H. Champliaud, M. Jahazi, Mat. Sc. Eng. A, 749 (2019).

[20] K.P. Mehta, P. Carlone, A. Astarita, F. Scherillo, F . Rubino, P. Vora, Mater Sci Eng A, 759 (2019).

[21] P. Cavaliere, A. De Santis, F. Panella, A. Squillace, Effect of welding parameters on mechanical and microstructural properties of dissimilar AA6082–AA2024 joints produced by friction stir welding **,** Mater Des, 30 (2009), pp. 609-616.

[22] V. Msomi, S. Mabuwa, Analysis of material positioning towards microstructure of the friction stir processed AA1050/AA6082 dissimilar joint, *Advances in Industrial and Manufacturing Engineering*, *1(2020)*, p.100002.

[23]M. Paidar, R.V. Vignesh, A. Khorram, O.O. Ojo, A. Rasoulpouraghdam, I. Pustokhina, Dissimilar modified friction stir clinching of AA2024-AA6061 aluminum alloys: effects of materials positioning, J Mater Res Technol, 9 (2020), pp. 6037-6047.

[24] H. K. Pabandi, H.R. Jashnani, M. Paidar, Effect of precipitation hardening heat treatment on mechanical and microstructure features of dissimilar friction stir welded AA2024-T6 and AA6061-T6 alloys, J Manuf Processes, 31 (2018), pp. 214-220.

[25] S. Mabuwa, V. Msomi, The effect of friction stir processing on the friction stir welded AA1050-H14 and AA6082-T6 joints, *Materials Today: Proceedings*, *26(2020)*, pp.193-199.

[26] O. Muribwathoho, V. Msomi, S. Mabuwa, A. Merdji, The mechanical properties of AA6082/AA1050 dissimilar joints subjected to multi-pass friction stir processing, *Engineering Research Express 3*, *3*(2021), p.035012.

[27] O. Muribwathoho, V. Msomi, S. Mabuwa, S.S. Motshwanedi, Impact of multi-pass friction stir processing on microhardness of AA1050/AA6082 dissimilar joints, *Materials Today: Proceedings*, *46 (2021)*, pp.651-657.

[28] S. Mabuwa, V. Msomi, Fatigue behaviour of the multi-pass friction stir processed AA8011-H14 and AA6082-T651 dissimilar joints, Eng. Fail. Anal, 118(2020), p.104876

[29] J. John, S.P. Shanmughanatan, M.B Kiran, Effect of tool geometry on microstructure and mechanical Properties of friction stir processed AA2024-T351 aluminium alloy, Mater. Today Proc, 5(2018), pp.2965–79.

[30] A. Kar, S. Suwas, S.V Kailas, Two-pass friction stir welding of aluminum alloy to titanium alloy: a simultaneous improvement in mechanical propertie, Materials Science and Engineering, A 733 (2018), pp.199–210.

[31] R. Sathiskumar, I. Dinaharan, N. Murugan S.J. Vijay, Influence of tool rotational speed on microstructure and sliding wear behavior of Cu/B4C surface composite synthesized by friction stir processing, Transactions of Nonferrous Metals Society of China, 25 (2015), pp.95–102

[32] S.R. Sharma, Z.Y. Ma, R.S Mishra, Effect of friction stir processing on fatigue behavior of A356 alloy, *Scripta Materialia 51*, *3*(2004), pp.237-241.

[33] K.J. Al-Fadhalah, A.I. Almazrouee, A.S. Aloraier, Microstructure and mechanical properties of multi-pass friction stir processed aluminium alloy 6063, *Materials & Design*, *53(2014)*, pp.550-560.

[34] R.S. Mishra, P.S. De, N. Kumar, Friction stir processing. In Friction stir welding and processing, *Springer International Publishing, Switzerland*, (2014), pp. 259-296.

[35] S. Mabuwa, V. Msomi, Effect of friction stir processing on gas tungsten arc-welded and friction stir-welded 5083-H111 aluminium alloy joints, *Advances in Materials Science and Engineering*, (2019), pp1-15.

[36] M.D. Sameer, A.K Birru, Mechanical and metallurgical properties of friction stir welded dissimilar joints of AZ91 magnesium alloy and AA 6082-T6 aluminium alloy, *Journal of Magnesium and Alloys 7*,2(2019), pp.264-271.

[37] M. Orłowska, T. Brynk, A. Hütter, J. Goliński, N. Enzinger, L. Olejnik, M. Lewandowska, Similar and dissimilar welds of ultrafine grained aluminium obtained by friction stir welding, *Materials Science and Engineering, A 777(2020)*, p.139076.

[38] M. Shunmugasundaram, A.P Kumar, L.P. Sankar, S. Sivasankar, S, Optimization of process parameters of friction stir welded dissimilar AA6063 and AA5052 aluminium alloys by Taguchi technique, *Materials Today: Proceedings27*, *2 (2020)*, pp.871-876.

[39] J. John, S.P. Shanmughanatan, M.B, Kiran, Effect of tool geometry on microstructure and mechanical Properties of friction stir processed AA2024-T351 aluminium alloy, Mater. Today Proc, 5(2018), pp. 2965–79.

[40] M. Paidar, R.V. Vignesh, A. Khorram, O.O. Ojo, A. Rasoulpouraghdam, I. Pustokhina, Dissimilar modified friction stir clinching of AA2024-AA6061 aluminum alloys: Effects of materials positioning, Journal of Materials Research and Technology, 9 (2020), pp.6037–47.

[41] G. Peng, Y. Ma, J. Hu, W. Jiang, Y. Huan, Z. Chen, T. Zhang, Nanoindentation hardness distribution and strain field and fracture evolution in dissimilar friction stir-welded AA 6061-AA 5A06 aluminium alloy joints, Advances in Material Science. and Engineering, (2018), pp.1–11.

[42] F. Khodabakhshi, A. Simchi, A.H, Kokabi , A.P Gerlich, Friction stir processing of an aluminum-magnesium alloy with pre-placing elemental titanium powder: in-situ formation of an Al3Ti-reinforced nanocomposite and materials characterization, Mater. Charact. 108 (2015) 102–14

[43] Y.C. Chen, J.C. Feng, H.J. Liu,Precipitate evolution in friction stir welding of 2219-T6 aluminium alloys,*Materials characterization 60*, *6* (2009), pp.476-481.

[44] M.M El-Rayes, E.A El-Danaf, The influence of multi-pass friction stir processing on the microstructural and mechanical properties of Aluminium Alloy 6082, *Journal of Materials Processing Technology 212*, *5*(2012),pp.1157-1168.

[45] M.S. Węglowski, P. Sędek, C. Hamilton,The effect of process parameters on residual stress in a friction stir processed cast aluminium alloy AlSi9Mg, *Engineering Transactions64*, *3*(2016), pp.301-309.

[46] S. Mabuwa, V. Msomi, V, Comparative analysis between normal and submerged friction stir processed friction stir welded dissimilar aluminium alloy joints, *Journal of Materials Research and Technology 9*, *5*(2020), pp.9632-9644.